

Regular-dimerized stack and neutral-ionic interfaces in mixed-stack organic charge-transfer crystals

A. Girlando and A. Painelli

Department of Chemical Physics, The University of Padua, 2 via Loredan, I-35131 Padova, Italy

(Received 19 February 1986)

Using diagrammatic valence-bond calculations, we have investigated the interplay between neutral-ionic (N - I) and regular-dimerized stack interfaces in mixed-stack organic charge-transfer (CT) crystals. The interactions relevant to the above two interfaces, that is, the intersite Coulomb and the electron-lattice phonon couplings, are introduced *via* a mean-field approach and a perturbative Herzberg-Teller expansion, respectively. The $\mathbf{k}=0$ results for finite chains (up to $\mathcal{N}=12$ sites) and rings (up to $\mathcal{N}=14$ sites) are extrapolated to $\mathcal{N}\rightarrow\infty$, obtaining an appropriate description of the electronic structure of a mixed, regular chain. The calculations distinguish the N and I phases as characterized, respectively, by nondegenerate and degenerate *singlet* ground states, the crossing point being found at a degree of ionicity (ρ) of about 0.63. Also the singlet-triplet gap vanishes in the I phase. The explicit consideration of the intersite Coulomb interactions changes the N - I interface from a continuous to a discontinuous one (first-order phase transition), whereas the electron-lattice phonon coupling makes the singlet degenerate (or quasidegenerate) ground state subject to the Peierls instability. The results are summarized in terms of a three-dimensional phase diagram relating ρ , the lattice-distortion energy, and the stabilization energy of the ionic stack due to intersite Coulomb interactions. This phase diagram is shown to nicely account for several experimental observations relevant to mixed-stack CT crystals and to their phase transitions.

I. INTRODUCTION

Most organic charge-transfer (CT) crystals are characterized by a mixed-stack structure, with electron-donor (D) and -acceptor (A) molecules arranged alternately along the direction of the predominating CT interaction.¹ These quasi-one-dimensional systems are conveniently classified in terms of the degree of ionicity (ρ , the average charge on the molecular sites) and of the stack structure.² In fact, mixed-stack CT crystals can have either a neutral (or "quasineutral," N , conventionally defined as $\rho < 0.5$) or an ionic ("quasiionic," I , $\rho > 0.5$) ground state. Moreover, the stack can be either regular (RS), when each molecule has the same CT integral with its two neighbors along the chain, or dimerized (DS), when the integrals are different. The N - I interface has been generally discussed in terms of the intersite Coulomb interactions,³⁻⁶ whereas one-electron pictures have been always used to investigate the role of electron-phonon coupling in determining the stack structure.^{7,8}

From the experimental side, it is interesting to note that N crystals generally have a RS structure, whereas the I ones easily undergo stack dimerization.⁹ Moreover, in the N - I phase transitions studied so far,^{10,11} the abrupt change in ρ is accompanied by the dimerization of the chain. It then appears that there is a rather strict interplay between N - I and RS-DS interfaces, and that both intersite Coulomb and electron-phonon interactions have to be taken into account to obtain a realistic phase diagram of mixed stack CT crystals. The aim of the present paper is to take a first step in this direction, by calculating the electronic structure of an isolated, regular

$\cdots DADAD \cdots$ chain.

Several models have been devised for the solution of the electronic problem of one-dimensional systems. The one-electron approximation adopted in the description of the electronic structure of conducting polymers¹² is not suited to the molecular crystals we are interested in, where electron-electron interactions are usually comparable with or larger than the bandwidths. Models neglecting the spin degrees of freedom³ can be solved analytically, but, as we shall see in the following, miss important aspects of the problem. In the present paper we have therefore chosen a numerical approach, the valence-bond (VB) technique proposed earlier by Soos and Mazumdar,⁵ which can take into account intrasite and intersite electron-electron interactions and the spin degrees of freedom.

The paper is organized as follows. The electronic Hamiltonian and its mean-field solution are described in Secs. II and III. Section IV introduces perturbatively the electron-lattice-phonon coupling and investigates the stability of the regular chain towards dimerization. Finally, in Sec. V we examine the effect of intersite Coulomb interactions on the N - I interface, and its interplay with the RS-DS one.

II. VALENCE-BOND ANALYSIS: HAMILTONIAN AND EXTRAPOLATION METHODS

The general Hamiltonian for an isolated DA regular chain can be easily written if one considers only one Wannier orbital per site and assumes that only the nearest-neighbor CT integral t is different from zero.¹³

$$\mathcal{H} = \sum_{i \text{ odd}} [-\varepsilon_D + U_D(\hat{n}_i + 1)/2](\hat{n}_i - 2) + \sum_{i \text{ even}} [-\varepsilon_A + U_A(\hat{n}_i - 1)/2]\hat{n}_i + t \sum_{i,\sigma} (a_{i,\sigma}^\dagger a_{i+1,\sigma} + a_{i+1,\sigma}^\dagger a_{i,\sigma}) + \sum_{\substack{i,j \\ i>j}} V_{ij} \hat{\rho}_i \hat{\rho}_j, \quad (1)$$

where i counts the \mathcal{N} molecular sites (odd for the D and even for the A sites), and σ the two spin states (α, β). The Fermi creation (annihilation) operator of an electron with spin σ at the i th site is indicated by $a_{i,\sigma}^\dagger$ ($a_{i,\sigma}$), whereas $\hat{n}_i = \sum_{\sigma} a_{i,\sigma}^\dagger a_{i,\sigma}$ is the occupation-number operator. The energies of the Wannier orbitals at D and A sites are ε_D and ε_A , respectively, U_D and U_A being the corresponding on-site (Hubbard) Coulomb interactions: The first ionization potential of D is $I_D = \varepsilon_D - U_D$, whereas the electron affinity of A is $A_A = \varepsilon_A$. Finally, $V_{i,j}$ is the Coulomb interaction between fully ionic i and j sites, and $\hat{\rho}_i$ is the charge operator, defined, as $\hat{\rho}_i = 2 - \hat{n}_i$ at D sites and $\hat{\rho}_i = \hat{n}_i$ at A sites.

For finite chains, the Hamiltonian (1) can be directly solved by the diagrammatic VB technique.¹⁴ On the other hand, a mean-field approximation for the intersite Coulomb interactions considerably simplifies the problem, yielding at the same time a first, physically significant description of the system. In the chosen mean-field approximation and by excluding the high-energy states with doubly ionized sites (D^{2+} and A^{2-}), the Hamiltonian (1) reads

$$\mathcal{H} = -\varepsilon \sum_i (-1)^i \hat{n}_i + t \sum_{i,\sigma} (a_{i,\sigma}^\dagger a_{i+1,\sigma} + a_{i+1,\sigma}^\dagger a_{i,\sigma}), \quad (2)$$

where the on-site energy ε is renormalized to give half the energy required to destroy an ionic pair:⁵

$$\varepsilon = (A_A - I_D + V)/2 + V\rho(\alpha - 1). \quad (3)$$

V is the Coulomb interaction in an isolated D^+A^- pair, α the Madelung constant, and ρ the degree of ionicity ($\rho = \langle \hat{\rho}_i \rangle$). The second term of Eq. (3) represents the Madelung energy per DA pair embedded in a lattice with charge ρ .

Besides providing a direct comparison with previous results,⁵ the main advantage of the mean-field approach is that the results can be expressed in terms of a single microscopic parameter, $z = \varepsilon/\sqrt{2}|t|$. By measuring the energies in $\sqrt{2}|t|$ units one obtains the following dimensionless Hamiltonian:

$$h = -z \sum_i (-1)^i \hat{n}_i - 2^{-1/2} \sum_{i,\sigma} (a_{i,\sigma}^\dagger a_{i+1,\sigma} + a_{i+1,\sigma}^\dagger a_{i,\sigma}). \quad (4)$$

Since the VB basis rapidly increases with \mathcal{N} , the required solution of (4) for the infinite stack can be found only by extrapolating to $\mathcal{N} \rightarrow \infty$ the results relevant to finite systems of increasing size. Results for DA rings with $\mathcal{N} \leq 10$ sites have been already reported.⁵ The rings were chosen instead of the open chains in order to minimize the end effects; however, the translational symmetry relevant to a *segregated* stack (C_{1v}) was adopted.⁵ Besides extending the calculations up to $\mathcal{N} = 14$ and to a larger range of z values, in the present paper we make use of the full translational and reflection symmetry of the DA rings (C_{nv} point group, with $n = \mathcal{N}/2$), and calculate all the

eigenstates of $\mathbf{k} = \mathbf{0}$ wave vector (A_1 and A_2 symmetry). As will be shown below, in this way additional and new insights are reached on the nature of the eigenstates and on the N -I and RS-DS interfaces.

Although the calculations for open chains are affected by the end effects, for $\mathcal{N} \rightarrow \infty$ they should tend to the same limit as the rings. Therefore, even if the advantages offered by the symmetry classification are lost, the consideration of the open chains in addition to the rings considerably helps the extrapolation process, giving more confidence to the final results. In the case of the energies and of the degree of ionicity, independent extrapolations for rings and open chains indeed yield practically identical values.

Recognizing that odd ($n = \mathcal{N}/2$ odd) and even rings converge differently, sometimes from opposite directions, to the limit value, the extrapolations have been carried out as follows.¹⁵ The data relevant to odd rings, even rings, and open chains have been separately least-squares-fitted to one of the following polynomials,

$$\begin{aligned} y(\mathcal{N}) &= y_\infty + a/\mathcal{N} + b/\mathcal{N}^2, \\ y(\mathcal{N}) &= y_\infty + a/\mathcal{N}^2 + b/\mathcal{N}^4, \\ y(\mathcal{N}) &= y_\infty + a/\mathcal{N} + b/\mathcal{N}^3, \end{aligned} \quad (5)$$

constraining y_∞ to be the same for the three groups of data. The Marquardt algorithm¹⁶ has been used in the fitting process. Only few interactions (four or five) were necessary to obtain the convergence (convergence criterion 10^{-10}) and the results are little affected by the choice of the fitting function (5).

The calculations have been carried out on a VAX 11/780 computer with 4 megabytes of core memory. The original VB programs¹⁴ were kindly given to us by Soos; they have been slightly modified to exclude doubly ionized sites and to introduce the full symmetry of the rings.

III. GROUND-STATE PROPERTIES AND THE MAGNETIC GAP

By exploiting the full symmetry of the rings, C_{nv} , the singlet VB diagrams⁵ in the above described reduced basis set (three valence states per site) are combined to transform like the A_1 and A_2 representations. The corresponding matrices of the Hamiltonian (4) are then computed, for various z values (from -2.8 to 2.8 in 0.1 steps), and diagonalized either exactly to obtain all the eigenvalues and eigenvectors ($\mathcal{N} \leq 10$) or by means of the coordinate relaxation technique¹⁴ to provide at least the lowest eigenstates ($\mathcal{N} = 12, 14$). For the open chains, no symmetry reduction of the matrices is possible, so that the calculations have been limited to $\mathcal{N} = 8$ for the full set of eigenstates, whereas only the lowest ones have been obtained for $\mathcal{N} = 10$ and 12 .

Figure 1 exemplifies the results obtained for even rings, odd rings ($\mathcal{N}/2$ even or odd), and open chains. The figure reports the lowest A_1 and A_2 eigenvalues divided by

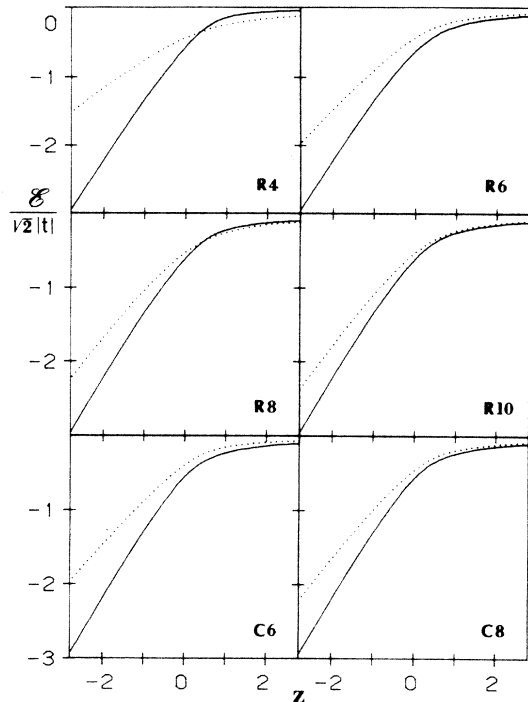


FIG. 1. Energy per site (\mathcal{E}) of rings (R) and open chains (C) with $\mathcal{N}=4-10$ and $\mathcal{N}=6,8$ sites, respectively, as a function of $z = \varepsilon/\sqrt{2}|t|$ [cf. Eq. (3)]. For rings, the solid and dotted lines distinguish the lowest-energy A_1 and A_2 singlets, respectively, whereas for open chains they indicate the two lowest-energy singlet eigenstates.

$\mathcal{N}(\mathcal{E}$, energy per site) as functions of z . We notice immediately that there is a marked difference in the $\mathcal{E}(z)$ behavior of even and odd rings. In fact, in even rings a crossing between A_1 and A_2 lowest energies per site occurs at $z = z^0(\mathcal{N})$, so that the symmetry of the ground state changes from A_1 to A_2 . No such crossing is observed in odd rings¹⁷ (or, as shown by Fig. 1, in open chains with any \mathcal{N}). On the other hand, physical intuition says that by letting $\mathcal{N} \rightarrow \infty$ the differences between even and odd rings must disappear.¹⁸ The properties evaluated for the two types of rings have to converge to the same value. Therefore either the even-ring crossing point $z^0(\mathcal{N})$ shifts towards infinity for $\mathcal{N} \rightarrow \infty$, or, beyond a certain critical z value (z_c), the ground state of the infinite chain becomes degenerate, the energies of A_1 and A_2 states tending to the same limit value for both even and odd rings.

A clear indication in favor of the second possibility comes from the behavior of the energy gap between the two lowest-energy singlet eigenstates. Figure 2 (upper part) shows the gap $\Delta_{SS}(\mathcal{N}, z)$ evaluated as $\mathcal{N}[\mathcal{E}_{A_1}(z) - \mathcal{E}_{A_2}(z)]$ for even and odd rings and as the difference between the two lowest eigenvalues for open chains. By extrapolating the three groups of curves as described in the preceding section, the $\mathcal{N} \rightarrow \infty$ gap reported in the lower part of Fig. 2 is obtained. The abrupt change of slope of the Fig. 2 curves suggests a nonasymptotic approach of the gap to zero. As a matter of fact, a

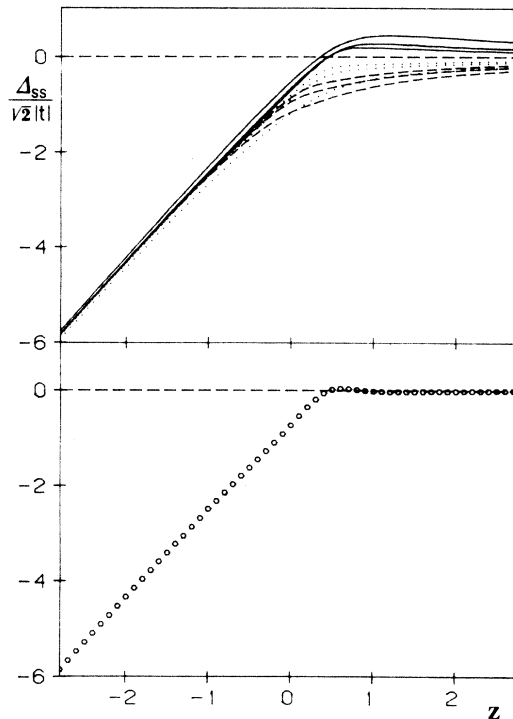


FIG. 2. Singlet-singlet energy gap (Δ_{SS}) vs z . Upper part: results for 4-, 8-, and 12-site rings (solid lines, convergence to the infinite-chain result from above); for 6-, 10-, and 14-site rings (dotted lines, convergence from below); and for 8-, 10-, and 12-site open chains (dashed lines, convergence from below). Lower part: infinite-chain extrapolated result.

z_c value can be estimated by fitting the $-0.2 \leq z \leq 0.4$ points of the $\Delta_{SS}(\infty, z)$ curve with a straight line: The result is $z_c = 0.42 \pm 0.03$. Practically the same value ($z_c = 0.43$) is obtained by using all the points from $z = -2.8$ to $z = 0.4$ and a parabola as a fitting function.¹⁹

The VB real-space approach adopted in this paper allows us to understand the physical meaning of the critical point. One can, in fact, observe that in the infinite-chain limit all the diagrams except the fully neutral one combine to give functions of both A_1 and A_2 symmetry. Therefore the A_1 and A_2 matrices become identical, apart from the presence in the A_1 matrix of the elements corresponding to the fully neutral VB diagram. On the other hand, as $\mathcal{N} \rightarrow \infty$ the fully neutral and fully ionic states are asymptotically decoupled.⁶ Thus z_c is the point where the contribution of the fully neutral diagram to the ground state vanishes and at the same time the fully ionic diagrams start to contribute. As a consequence, above z_c the lowest eigenstates of A_1 and A_2 symmetry are exactly degenerate. This degeneracy can be found only in models including the spin degrees of freedom: Only in this case, in fact, can the fully ionic structure be described by at least two equivalent “Kekulé-type” VB diagrams,⁵ differing only in the spin pairing between adjacent sites. We finally remark that the meaning, not only the value, of z_c is different from that of Ref. 5, where $z_c = 0.52$ was associated with a symmetry change of the ground-state eigenfunction at the $N-I$ interface. In the present work, in-

stead, z_c marks the point in which the *singlet* ground state becomes degenerate.

We defer to the next section the discussion on the consequences of the singlet degeneracy on the stability of the regular chain, and come back to the $\mathcal{N} \rightarrow \infty$ extrapolations of the ground-state energy per site, \mathcal{E}_G . Such extrapolations, performed separately on rings and open chains, converge to practically the same value: in Table I we have reported part of the obtained $\mathcal{E}_G(\infty, z)$, giving as significant digits those common to the two extrapolations. The corresponding $\Delta_{SS}(\infty, z)$ are given in column 3. We notice that the reported values of \mathcal{E}_G do not differ appreciably from the previous ones,⁵ despite the fact that the ground states of the odd rings were incorrectly given.¹⁷

A microscopic parameter fundamental to the description of mixed-stack CT crystals is the degree of ionicity ρ , as it reflects the mixing between *D* and *A* orbitals (i.e., the strength of the CT interaction). Moreover, being directly measurable,^{9,20} it provides a convenient link between theory and experiment. In the present calculations ρ could be evaluated from the ground-state eigenvector as the expectation value of the charge operator. We follow instead a simpler route, based on the relationship between ρ and the first derivative of \mathcal{E}_G with respect to z :^{5,6}

$$\rho = 1 - (\sqrt{2} |t|)^{-1} \left[\frac{\partial \mathcal{E}_G}{\partial z} \right]. \quad (6)$$

Figure 3 (upper part) reports ρ as a function of z for rings and open chains with various \mathcal{N} values. Whereas for even rings a discontinuity in the z dependence occurs

at the crossing point $z^0(\mathcal{N})$ (in correspondence with the change in the ground-state symmetry) in odd rings and in open chains the $\rho(z)$ function is well behaved. The $\mathcal{N} \rightarrow \infty$ extrapolated $\rho(z)$ is shown in the lower part of Fig. 3; part of the numerical values are reported in column 4 of Table I.²¹ Since the intersite Coulomb interactions are not explicitly accounted for, collective effects cannot show up and no discontinuity is observed in the $\rho(z)$ curve of the infinite chain. Only a maximum in $\partial\rho/\partial z$ is found at z_c , indicating a continuous passage from the *N* to *I* regime (i.e., from a ground state without a contribution from the fully ionic diagrams to one without a contribution from the fully neutral diagram). The value marking the passage is $\rho_c \simeq 0.63$: The asymmetry of the *N-I* interface is again attributable to the spin degrees of freedom.⁵

We conclude this section by briefly looking at the singlet-triplet gap, which determines the magnetic properties of the system.⁵ The symmetry of the rings has not been exploited in the triplet-state calculations, which have been carried out up to $\mathcal{N}=12$ for both rings and open chains. The singlet-triplet gap Δ_{ST} has then been determined by

$$\Delta_{ST}(\mathcal{N}, z) = \mathcal{N} [\mathcal{E}_G(z) - \mathcal{E}_T(z)],$$

where \mathcal{E}_G and \mathcal{E}_T are the lowest singlet and triplet energies per site, respectively. The results are similar to those of the singlet-singlet gap (Fig. 2); that is, after an almost straight line of slope ~ 2 , Δ_{ST} tends to become zero. In this case, however, with increasing \mathcal{N} , Δ_{ST} tends to zero

TABLE I. Infinite-chain extrapolated values ($\sqrt{2} |t|$ units) of ground-state energy per site (\mathcal{E}_G), singlet-singlet gap (Δ_{SS}), degree of ionicity (ρ), and singlet-triplet gap (Δ_{ST}). This table reports only a significant sample of the calculated values; except for Δ_{ST} , all the other parameters have been evaluated in 0.1 z steps from -2.8 to 2.8 .

z	\mathcal{E}_G	Δ_{SS}	ρ	Δ_{ST}
-2.8	-2.964 29	-5.86		-5.87
-2.4	-2.586 81	-5.09	0.0634	-5.11
-2.0	-2.215 71	-4.33	0.0820	-4.36
-1.6	-1.853 63	-3.59	0.1085	-3.62
-1.2	-1.504 6	-2.86	0.1483	-2.90
-0.8	-1.174 7	-2.15	0.2061	-2.21
-0.4	-0.873 1	-1.45	0.291	-1.55
0.0	-0.610 9	-0.73	0.40	
0.1	-0.552 6	-0.54	0.43	-0.67
0.2	-0.498	-0.36	0.47	-0.43
0.3	-0.448	-0.19	0.532	-0.28
0.4	-0.406	-0.06	0.613	-0.14
0.5	-0.370 2	0.01	0.6930	-0.05
0.6	-0.341 7	0.04	0.7371	-0.02
0.7	-0.317 1	0.03	0.7706	-0.01
0.8	-0.295 6	0.01	0.7979	0.00
1.2	-0.230 47	-0.04	0.8689	0.00
1.6	-1.187 05	-0.03	0.9102	0.00
2.0	-0.156 46	-0.02	0.9349	0.00
2.4	-0.134 03	-0.02	0.9518	0.00
2.8	-0.116 95	-0.01		0.00

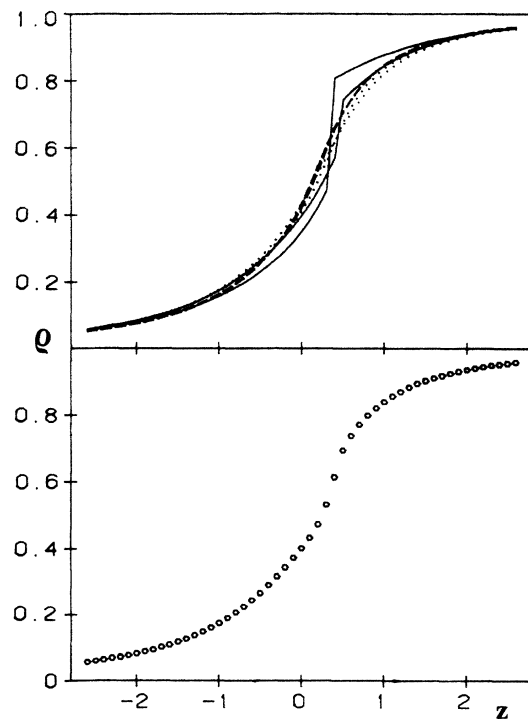


FIG. 3. Degree of ionicity (ρ) vs z . Upper part: results for 4- and 8-site rings (solid lines); for 6- and 10-site rings (dotted lines); and for 6- and 8-site open chains (dashed lines). Lower part: infinite-chain extrapolated result.

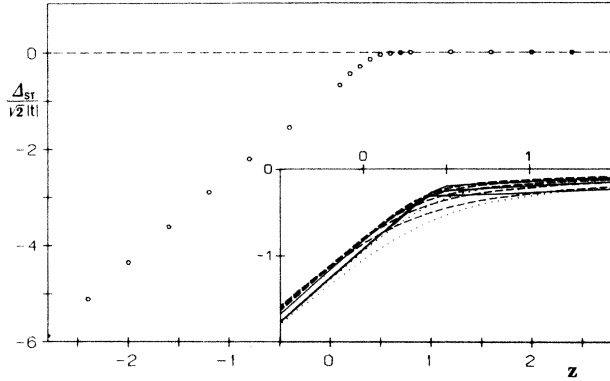


FIG. 4. Singlet-triplet energy gap (Δ_{ST}) vs z , in the infinite-chain limit. The inset shows the results for finite-size even rings (solid lines), odd rings (dotted lines), and open chains (dashed lines), all converging from below to the infinite-chain limit.

always from below (Fig. 4, inset) rather than from two opposite directions, depending on the ring type, as was observed for Δ_{SS} (Fig. 2, upper part). As a consequence, the $\mathcal{N} \rightarrow \infty$ extrapolation of Δ_{ST} is less bound than in the Δ_{SS} case, and the determination of a finite z_c for the vanishing of Δ_{ST} is less safe. In any case, the extrapolated Δ_{ST} values (reported in Fig. 4 and in the last column of Table I) go to zero at $z_c \simeq 0.47 \pm 0.05$ ($\rho_c = 0.67$), which we believe is not significantly different from that relevant to Δ_{SS} . Moreover, the close similarity of $\Delta_{SS}(\infty, z)$ and $\Delta_{ST}(\infty, z)$ (Table I and Figs. 2 and 4) indicates that the first-excited singlet and triplet states are degenerate or quasidegenerate in the full z range. Exact degeneracy can indeed be expected in the $z \rightarrow \pm\infty$ limits: for $t \rightarrow 0$ the electron on a site cannot know if those on the nearest-neighbor sites have parallel or antiparallel spin.

We therefore agree with the previous conclusion⁵ that the magnetic gap of a mixed regular chain vanishes in the ionic regime. However, the observation of activated magnetic susceptibility in a mixed-stack crystal does not necessarily imply that the system is on the neutral side. In fact, in the ionic side the singlet ground state is degenerate; thus, as shown in the next section, the regular chain tends to dimerize, opening a finite magnetic gap.

IV. REGULAR-DIMERIZED STACK INTERFACE

We now focus attention on the consequences that the singlet ground-state degeneracy (or quasidegeneracy) can have on the stability of a regular mixed chain. It is, in fact, quite obvious that the degenerate system is unstable against any perturbation which, lowering the symmetry, allows the mixing of the A_1 and A_2 states. The most likely perturbation is the coupling of the electrons to the lattice phonons, which leads to the well-known Peierls-type instability of one-dimensional systems.^{22–24} The relevant phonons are in this case the $\mathbf{k}=0$ optical ones (A_2 symmetry), corresponding to the zone-boundary phonons causing the Peierls instability in the isoelectronic

half-filled segregated stack system. For the sake of simplicity, and without loss of generality, we consider just one translational phonon,

$$u = \left[\frac{2}{\mathcal{N}} \right]^{1/2} \sum_{i \text{ odd}} u_i = \left[\frac{2}{\mathcal{N}} \right]^{1/2} \sum_{i \text{ odd}} (x_i - x_{i+1}), \quad (7)$$

where x_i is the mass-weighted longitudinal displacement of the i th molecule. The coupling of the phonon to the electron system takes place through a modulation of the CT integrals. For small displacements the u_i dependence of the CT integral between the i and $i+1$ sites (t_i) can be linearized as

$$t_i = t + \left[\frac{\partial t_i}{\partial u_i} \right]_0 u_i, \quad (8)$$

where t is the CT integral of the regular chain. It is then convenient to define the linear electron-phonon coupling constant g_{ph} as ($\hbar=1$)

$$g_{\text{ph}} = \frac{2}{(2\omega_{\text{ph}})^{1/2}} \left[\frac{\partial t_i}{\partial u_i} \right]_0, \quad (9)$$

where ω_{ph} is the phonon frequency.

If one allows for the t variation, the mean-field electronic Hamiltonian of the mixed chain is

$$\mathcal{H} = -\varepsilon \sum_i (-1)^i \hat{n}_i + \sum_{i,\sigma} t_i (a_{i,\sigma}^\dagger a_{i+1,\sigma} + a_{i+1,\sigma}^\dagger a_{i,\sigma}). \quad (10)$$

Equations (8)–(10) yield

$$\begin{aligned} \mathcal{H} = & -\varepsilon \sum_i (-1)^i \hat{n}_i + t \sum_{i,\sigma} (a_{i,\sigma}^\dagger a_{i+1,\sigma} + a_{i+1,\sigma}^\dagger a_{i,\sigma}) \\ & - (\mathcal{N}\omega_{\text{ph}})^{1/2} g_{\text{ph}} u \mathcal{B} = \mathcal{H}_e + \mathcal{H}_{e-\text{ph}}, \end{aligned} \quad (11)$$

where \mathcal{B} is the bond-order alternation operator:

$$\mathcal{B} = \mathcal{N}^{-1} \sum_{i,\sigma} (-1)^i (a_{i,\sigma}^\dagger a_{i+1,\sigma} + a_{i+1,\sigma}^\dagger a_{i,\sigma}). \quad (12)$$

\mathcal{H}_e and $\mathcal{H}_{e-\text{ph}}$ are the rigid-lattice electronic Hamiltonian of Eq. (4) and the electron-phonon coupling term.

The usual Peierls-type treatment^{22–24} would require knowledge of the dependence of the ground-state electronic energy from u . One could tackle the problem by calculating, *via* the VB technique, this energy for various u values, i.e., various distorted chains. This route is clearly very laborious, requiring a high number of calculations. On the other hand, if one is only interested in what happens before the chain distortion occurs, one can adopt the much simpler ‘‘Kohn-anomaly’’ approach.²³ The problem is then reduced to the evaluation (*via* a perturbative approach in terms of $\mathcal{H}_{e-\text{ph}}$) of the effect of the electron system on the phonon dynamics. The relevant expression for the renormalized phonon frequency can be obtained by various methods; here we shall adopt the one²⁵ which allows us to understand better the different behavior of finite open chains and rings.

In the proximity of $u=0$, the dependence of the ground-state energy $E_G(u)$ from u can be expressed by a Herzberg-Teller expansion around such a point:

$$\begin{aligned}
E_G(u) &= E_G + \langle G | \mathcal{H}_{e-\text{ph}} | G \rangle - \sum_F \frac{|\langle G | \mathcal{H}_{e-\text{ph}} | F \rangle|^2}{E_F - E_G} \\
&= E_G - (\mathcal{N}\omega_{\text{ph}})^{1/2} g_{\text{ph}} u \langle G | \mathcal{B} | G \rangle - \mathcal{N}\omega_{\text{ph}} u^2 g_{\text{ph}}^2 \sum_F \frac{|\langle G | \mathcal{B} | F \rangle|^2}{E_F - E_G},
\end{aligned} \tag{13}$$

where $|G\rangle$ and $|F\rangle$ represent, respectively, the lowest and the excited eigenstates of \mathcal{H}_e , with energy E_G and E_F , respectively. The first and second derivatives of the total energy, $E_{TO}(u) = E_G(u) + \omega_{\text{ph}}^2 u^2/2$, with respect to u , give the equilibrium position of the chain and its vibrational frequency. At $u=0$ the first derivative is zero only if the term $\langle G | \mathcal{B} | G \rangle$ is zero. For rings, which have the full symmetry of the infinite chain, this condition is satisfied by symmetry, \mathcal{B} being an antisymmetric operator. On the other hand, this argument does not apply to finite open chains; in such a case the position $u=0$ (regular chain) is *not* an equilibrium position for the system.²⁶ The condition $\langle G | \mathcal{B} | G \rangle = 0$ must, of course, be regained also for open chains in the limit $\mathcal{N} \rightarrow \infty$.

The renormalized phonon frequency Ω_{ph} of finite rings and open chains, given by the second derivative of E_{TO} with respect to u , is in any case obtained as²³

$$\Omega_{\text{ph}}^2 = \omega_{\text{ph}}^2 - \omega_{\text{ph}} g_{\text{ph}}^2 \mathcal{N} \chi_b, \tag{14}$$

where χ_b , defined by

$$\chi_b = 2 \sum_F \frac{|\langle G | \mathcal{B} | F \rangle|^2}{E_F - E_G}, \tag{15}$$

expresses the electronic response to the phonon perturbation.

The coupling with the electron system softens the lattice phonon frequency; when it reaches zero the displacement along u costs no energy, and the regular mixed-stack chain dimerizes. The borderline between regular and dimerized stack stability regions is then given by

$$\chi_b^{-1} = \mathcal{N} \mathcal{E}_D. \tag{16}$$

In Eq. (16), $\mathcal{E}_D = g_{\text{ph}}^2/\omega_{\text{ph}}$ ($= \sum_{\text{ph}} g_{\text{ph}}^2/\omega_{\text{ph}}$, if more than one phonon is involved) is the lattice distortion energy per unit cell.²⁷ It represents the electronic energy gain due to the lattice relaxation when the bond orders change from uniform ($\langle \mathcal{B} \rangle = 0$) to perfectly alternating ($\langle \mathcal{B} \rangle = 1$). In this respect, \mathcal{E}_D plays the same role as the small polaron binding energy does in the case of electron-intramolecular phonon coupling.²⁸

The electronic response χ_b [Eq. (15)] can be easily obtained as a function of z (or ρ) by applying the operator \mathcal{B} of Eq. (12) to the eigenvectors obtained by the calculations of the preceding section. The resulting $(\mathcal{N}\chi_b)^{-1}$ are reported ($\sqrt{2}|t|$ units) in the upper part of Fig. 5 and are limited to rings up to $\mathcal{N}=10$ and to open chains up to $\mathcal{N}=8$, since only in these cases has the full set of eigenvectors to be used in Eq. (15) been obtained. From the figure it is evident that even- and odd-ring curves converge to the $\mathcal{N} \rightarrow \infty$ result from opposite directions (at least for $\rho \leq 0.8$). The shapes of the curves relevant to the open chains are instead qualitatively different. This ap-

parently anomalous behavior can be understood if we define the following "asymmetry parameter" ϕ :

$$\phi = \frac{2}{\mathcal{N}} \sum_{i \text{ odd}} \frac{t_i - t_{i+1}}{t_i + t_{i+1}}. \tag{17}$$

In the case of rings, $\phi=0$ and 1 in the opposite limits of a regular and of a fully alternating (i.e., isolated dimers) arrangement of D and A sites. If the isolated dimers form an open chain, again $\phi=1$. However, a regular open chain has $\phi = (\mathcal{N}-1)^{-1}$, since $t_i = 0$. Once more, the full symmetry result ($\phi=0$), is regained only in the limit $\mathcal{N} \rightarrow \infty$. For finite \mathcal{N} , therefore, the open chains are expected to exhibit a behavior intermediate between that of an isolated dimer and that of a regular ring, tending to the latter with increasing \mathcal{N} . For an isolated dimer, Eq. (15) easily gives the analytical result²⁵

$$(\sqrt{2}|t|\mathcal{N}\chi_b)^{-1} = \{2(2\rho-1)^2[\rho(1-\rho)]^{1/2}\}^{-1}.$$

Such a function tends to infinity for $\rho=0.5$ (as well as for

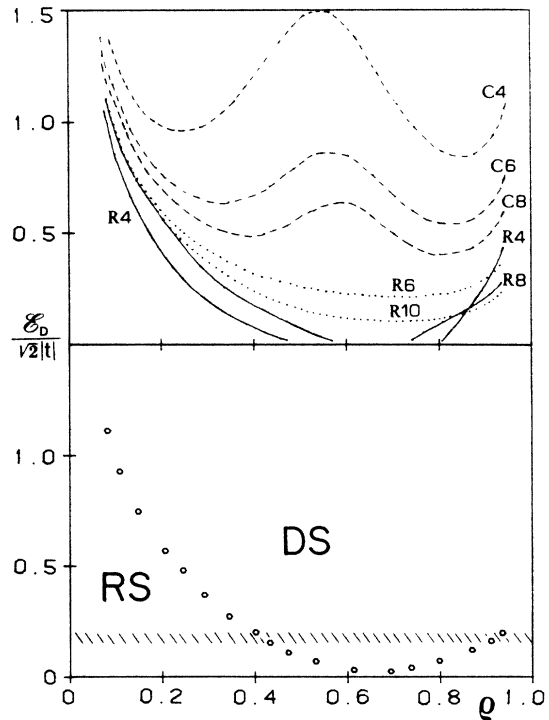


FIG. 5. Regular-stack (RS) and dimerized-stack (DS) stability regions [cf. Eq. (16) in the text]. \mathcal{E}_D is the lattice-distortion energy per site and ρ the degree of ionicity. Upper part: results for (4–10)-site rings (R) and (4–8)-site open chains (C). Lower part: infinite-chain limit; the dashed area represents an experimentally plausible range of values for $\mathcal{E}_D/\sqrt{2}|t|$ in organic CT crystals.

$\rho=0$ and 1) and is symmetric around such a value, with two minima at $\rho=0.15$ and 0.85 . In Fig. 5 one can see how the open chains progressively depart from such behavior with increasing \mathcal{N} , the $\mathcal{N}=4$ curve being already rather different from the dimer case (asymmetric and not going to infinity for $\rho=0.5$). As stated above, the $\mathcal{N}\rightarrow\infty$ limit must be the same for chains and rings; we can therefore extrapolate the curves of the upper part of Fig. 5 as has been described in Sec. II. Since, however, only two data points are available for each of the two groups of even and odd rings, in such cases the extrapolating functions (5) have been limited to only two terms. The resulting curve for the infinite chain is reported in the lower part of Fig. 5.

Although it offers only a zero-temperature description, Fig. 5 can be used as a sort of phase diagram for the stability of regular stacks against dimerization. On the basis of the condition (16), regular chains are stable only below the curve of Fig. 5, and unstable above. The value of $\mathcal{E}_D/\sqrt{2}|t|$ is generally estimated²⁹ around 0.15 – 0.20 (dashed area); it is then nice to see that Fig. 5 immediately explains the experimental observations referred to in the Introduction. In fact, neutral chains ($\rho\leq 0.3$) have a regular structure also at low temperatures;⁹ as far as we know, mixed-regular-stack crystals with ρ between about 0.4 and 0.8 have not been observed;⁹ finally, ionic compounds with $\rho\geq 0.9$ are found to undergo a RS-DS phase transition by lowering the temperature.^{7,20,30} We predict that for the latter systems a $\mathbf{k}=0$ soft-phonon mode should be observable in the infrared spectra.

The dimerization instability described in this section cannot be directly associated with the widely investigated spin-Peierls instability of segregated-stack CT crystals.²⁴ In fact, in a mixed stack the difference of the on-site energies makes possible the double occupancy of the D sites even in the large- U limit. Additional insight into the physics of the phenomenon can be gained in terms of the real-space VB description of Peierls instabilities previously proposed for finite- U segregated stacks.³¹ It is easy to realize that the ground state of neutral or quasineutral mixed chains is mostly described by nonbonded VB diagrams, where doubly occupied D sites alternate along the stack with empty A sites. Such diagrams do not favor the chain distortion,³¹ so that a large stability range is expected for mixed stacks in the neutral regime, as confirmed by Fig. 5. When the ionicity increases, bonded diagrams begin to contribute to the ground state and, correspondingly, the system becomes less and less stable. In the largely ionic side, on the other hand, the stability is progressively regained due to the decrease of t . Only in the limit of large positive z ($\rho=1$), a mixed regular chain becomes equivalent to a large- U segregated stack.

V. NEUTRAL-IONIC VERSUS REGULAR-DIMERIZED STACK INSTABILITY

In the preceding section it has been shown that, due to electron–lattice-phonon coupling, regular-mixed-stack

chains with intermediate degrees of ionicity are strongly unstable against dimerization. This finding has been used to justify the fact that such CT crystals have not been experimentally found. On the other hand, it is known^{5,6} that the intersite Coulomb interaction (so far not explicitly considered) is also a source of instability for intermediate-charge chains, giving rise to an abrupt jump in ρ in going from neutral to ionic systems. It is then clear that these two interactions compete in pointing towards two different uneven charge distributions along the chain; the electron-phonon coupling tends to distort the chain, modulating the intersite electronic density (bond charge-density wave, B-CDW); on the other hand, the intersite Coulomb interaction favors the already present uneven electron distribution on the D and A sites (site charge-density wave, S-CDW).⁸ Any realistic model of mixed-stack CT crystals must therefore take into account both the above interactions.

The mean-field approach allows one to analyze the effects of the intersite Coulomb interactions on the $\rho(z)$ function by separating the contributions of the two terms in Eq. (3).⁵ One defines $\mathcal{E}_C = V(\alpha - 1)$ as the contribution given by intersite Coulomb interactions to the stabilization of a D^+A^- pair self-consistently embedded in the ionic lattice. Then, setting $f = \mathcal{E}_C/\sqrt{2}|t|$ and $z_0 = (A_A - I_D + V)/2\sqrt{2}|t|$, Eq. (3) in dimensionless form is rewritten as

$$z_0(z, f) = z - f\rho(z). \quad (18)$$

For a given value of f , z , and ρ , the curve $\rho(z)$ of the lower part of Fig. 3 can be used to compute z_0 , thus obtaining the ρ -versus- z_0 curves reported in Fig. 6 [actually, the abscissa axis reports $z_0 + f/2$ in order to keep the $\rho(z_0, f)$ curves in the same place for different f values.] By increasing f (that is, the importance of the intersite Coulomb interactions), the $f=0$, S-shaped curve of Fig. 3 becomes steeper. Beyond a critical $f_c = (\partial z/\partial \rho)_{z=z_c}$ (roughly estimated by our calculation as 1.3 ± 0.3) the $\rho(z_0)$ function is no longer single valued (Fig. 3, $f=3.5$). It is not difficult to realize that in such a case the curve

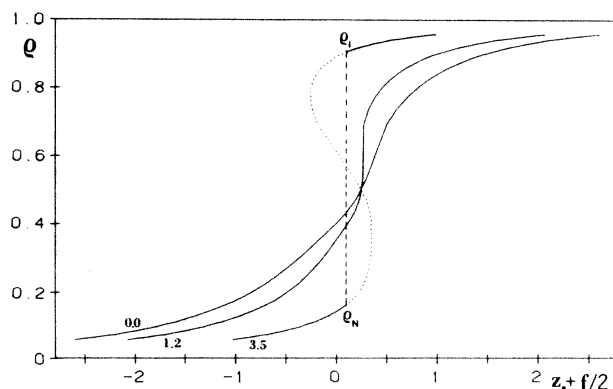


FIG. 6. Degree of ionicity (ρ) vs $z_0 + f/2$ for $f=0.0, 1.2$, and 3.5 . f [Eq. (18)] is a measure of the intersite Coulomb interaction; the $f=0.0$ curve is the infinite-chain extrapolation of Fig. 3, lower part. The geometrical construction on the $f=3.5$ curve is explained in the text.

interval with negative slope corresponds to *unstable* states.³² In fact, the energy as a function of ρ can be written as $\mathcal{E}_G(\rho) = z_0(1-\rho) + q(f, \rho)$, where $q(f, \rho)$ is some function of f and ρ . For the stability, the energy must be at a minimum; that is

$$\left(\frac{\partial^2 \mathcal{E}_G}{\partial \rho^2} \right)_{z_0, f} = \left(\frac{\partial^2 q}{\partial \rho^2} \right)_{z_0, f} > 0.$$

After some elementary algebra, one can rewrite the stability condition as

$$\left(\frac{\partial \rho}{\partial z_0} \right)_f = \left(\frac{\partial^2 q}{\partial \rho^2} \right)_{z_0, f}^{-1} > 0.$$

The stable equilibrium states can be derived, as usual, by tracing a tie line $\rho_N - \rho_I$ such as $\int_{\rho_N}^{\rho_I} \rho(z_0) dz_0 = 0$; that is, by using the well-known Maxwell equal-area (equal-energy) construction.³³ Therefore the *N-I* interface becomes discontinuous (first-order phase change) for $f > f_c$, the ρ values between ρ_N and ρ_I not representing stable states (the curve intervals within this ρ range and with positive slope correspond to metastable states, and those with negative slope to unstable states, as discussed above).

We are now in the position of modifying Fig. 5 to include the effect of intersite Coulomb interactions. Since f cannot be modulated by u , the ρ dependence of χ_b is not modified. Therefore the curve representing the RS-DS interface remains the same for $f \leq f_c$: For weak \mathcal{E}_C all the ρ values are allowed and the chain may undergo a second-order B-CDW instability. By increasing f beyond f_c , larger and larger ρ intervals become progressively forbidden, so that the Fig. 5 curve is progressively cut from below by the tie lines of Fig. 6, connecting ρ_N and ρ_I ; the results for some experimentally relevant⁶ f values are reported in Fig. 7. Then for appreciably large \mathcal{E}_C also first-order *N-I* (S-CDW) phase transitions become possible. Since, however, the $\rho_N - \rho_I$ tie lines are not parallel to

the abscissa axis, and a rather small \mathcal{E}_D is sufficient to induce the B-CDW instability, it is very likely that a *N-I* phase transition is accompanied by a stack dimerization.

The above considerations are conveniently illustrated by comparing the predictions of Fig. 7 with the experimental behavior of a CT crystal undergoing a *N-I* transition. The obvious choice is the tetrathiafulvalene-chloranil (TTF-CA) compound, whose temperature-induced *N-I* phase transition has been deeply investigated.^{10, 34-36} From these investigations we can extract the microscopic parameters needed to use Fig. 7. The Madelung-energy calculations³⁵ lead to an estimate $\mathcal{E}_C \simeq 0.8$ eV just above the phase transition; since t is evaluated to be ~ 0.24 eV,³⁶ we have $f \simeq 2.4$, corresponding to curve *b* in Fig. 7. Moreover, always just above the transition, $\rho \simeq 0.30-0.35$.⁹ If we assume the plausible value²⁹ of $0.15-0.20$ for $\mathcal{E}_D/\sqrt{2}|t|$, the system lies about at point *S* in the phase diagram. This point is below curve *b*; the stack should be regular, as indeed it is.³⁴ On the other hand, point *S* is on the edge of the *N-I* instability; a small increase of ρ brings it on the ionic side, and the phase transition is first-order, as recently found by Tokura *et al.*¹⁰ The first allowed ρ value is around 0.85; if $\mathcal{E}_D/\sqrt{2}|t|$ remains the same as in the neutral phase, the system would lie at point *R* in the phase diagram. However, *R* is now above the RS-DS instability curve, with the crossing occurring at *Q*; the ionic phase of TTF-CA is expected to be dimerized, as experimentally found³⁴ (of course, the actual ρ value of the ionic phase, ~ 0.64 ,^{9, 10} cannot be deduced from Fig. 7, which is relevant to the regular stacks only). Just one example is obviously not enough to assess the general validity of Fig. 7. However, the success in the explanation of the experimental data on the temperature-induced phase transition of TTF-CA indicates that the obtained phase diagram offers a physically significant picture of *N-I* and RS-DS interfaces in mixed-stack CT crystals.

VI. CONCLUSIONS

In this paper we have investigated the *N-I* and RS-DS interfaces of mixed-stack CT crystals. The adopted real-space VB approach yields a complete description of the electronic system, taking into account the spin degrees of freedom, the effects of the CT interaction, and the electron correlations. We have discovered that the singlet ground state of a regular chain becomes degenerate above a certain critical value of the degree of ionicity. This point marks the borderline between *N* and *I* ground states; most important, however, is the fact that in the region of the degeneracy (or quasidegeneracy) the chain is strongly unstable towards a Peierls distortion.

We have analyzed the Peierls instability by introducing the electron-lattice-phonon coupling through a Herzberg-Teller expansion of the VB ground-state energy. In this way the stability regions of the regular and dimerized stack phases have been delimited. Moreover, the interplay of the RS-DS with the *N-I* instability has been investigated. As a result, we have been able to construct a three-dimensional phase diagram, relating the lattice distortion energy, the Coulomb interaction energy, and the degree of ionicity. These quantities can be experimentally

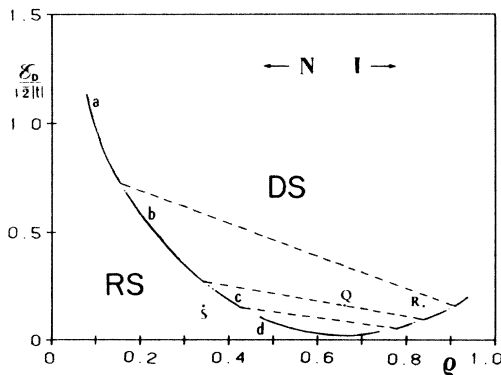


FIG. 7. Phase diagram for mixed-stack CT crystals. The *a*, *b*, *c*, and *d* curves correspond to $f = 3.5, 2.4, 1.2,$ and 0.0 (decreasing importance of the intersite Coulomb interactions); the dashed line (analogous to the tie line of Fig. 6) indicates the forbidden ρ region for the given f value. \mathcal{E}_D is the lattice distortion energy per site. The points *S*, *Q*, and *R* are explained in the text.

determined or reasonably estimated: The phase diagram is then shown to nicely account for the experimental behavior of the mixed-stack CT crystals investigated so far.

The achievements of the model give us confidence in the route undertaken. Extension of the present work will be in examining whether the RS-DS instability curve is appreciably modified when the Hamiltonian including the intersite Coulomb interactions is solved directly, rather than through a mean-field approach. Preliminary results suggest that this is not the case. It will also be interesting to investigate the effects of the electron-molecular vibration interaction, which has not been considered in the

present paper and which is known^{8,25} to influence the N - I instability.

ACKNOWLEDGMENTS

This work would not have been possible without the VB computer programs kindly given to us by Professor Z. G. Soos, and without his assistance in the first stages of use. We also acknowledge Professor Soos's stimulating correspondence. Thanks are due to Professor C. Pecile for his continuous encouragement. This work has been supported by the Ministry of Education (Ministero della Pubblica Istruzione) and by the National Research Council (Consiglio Nazionale delle Ricerche) of Italy.

- ¹F. H. Herbstein, in *Perspective in Structural Chemistry*, edited by J. P. Dunitz and J. A. Ibers (Wiley, New York, 1971), Vol. IV, p. 166.
- ²Z. G. Soos and D. J. Klein, in *Molecular Association*, edited by R. Foster (Academic, New York, 1975), Vol. 1, p. 1.
- ³J. D. Krugler, C. G. Montgomery, and H. M. McConnell, *J. Chem. Phys.* **41**, 2421 (1964). R. Bruinsma, P. Bak, and J. B. Torrance, *Phys. Rev. B* **27**, 456 (1983).
- ⁴P. J. Strelbel and Z. G. Soos, *J. Chem. Phys.* **53**, 4077 (1970).
- ⁵Z. G. Soos and S. Mazumdar, *Phys. Rev. B* **18**, 1991 (1978).
- ⁶Z. G. Soos and S. Kuwajima, *Chem. Phys. Lett.* **122**, 315 (1985).
- ⁷J. B. Torrance, J. J. Mayerle, and J. I. Crowley, *Bull. Am. Phys. Soc.* **23**, 425 (1978); A. Girlando, C. Pecile, and J. B. Torrance, *Solid State Commun.* **54**, 753 (1985).
- ⁸B. Horovitz and B. Schaub, *Phys. Rev. Lett.* **50**, 1942 (1983); B. Horovitz, *Mol. Cryst. Liq. Cryst.* **120**, 1 (1985).
- ⁹A. Girlando, A. Painelli, and C. Pecile, *Mol. Cryst. Liq. Cryst.* **120**, 17 (1985).
- ¹⁰A. Girlando, F. Marzola, C. Pecile, and J. B. Torrance, *J. Chem. Phys.* **79**, 1075 (1983); Y. Tokura, Y. Kaneko, H. Okamoto, S. Tanuma, T. Koda, T. Mitani, and G. Saito, *Mol. Cryst. Liq. Cryst.* **125**, 71 (1985).
- ¹¹A. Girlando, C. Pecile, A. Brillante, and K. Syassen, *Solid State Commun.* **57**, 891 (1986); Y. Tokura, H. Okamoto, T. Mitani, G. Saito, and T. Koda, *ibid.* **57**, 607 (1986).
- ¹²M. J. Rice and E. J. Mele, *Phys. Rev. Lett.* **49**, 1455 (1982).
- ¹³Z. G. Soos, R. H. Harding, and S. Ramasesha, *Mol. Cryst. Liq. Cryst.* **125**, 59 (1985).
- ¹⁴Z. G. Soos and S. Ramasesha, *Phys. Rev. B* **29**, 5410 (1984); S. Ramasesha and Z. G. Soos, *J. Chem. Phys.* **80**, 3278 (1984); *Int. J. Quantum Chem.* **25**, 1003 (1984).
- ¹⁵J. C. Bonner and H. W. J. Blöte, *Phys. Rev. B* **25**, 6959 (1982); Z. G. Soos, S. Kuwajima, and J. E. Mihalick, *ibid.* **32**, 3124 (1985).
- ¹⁶P. R. Bevington, *Data Reduction and Error Analysis for the Physical Sciences* (McGraw-Hill, New York, 1969), p. 235.
- ¹⁷As recently and independently recognized by Z. G. Soos (Ref. 6), the ground states of odd rings are incorrectly given in Ref. 5.
- ¹⁸S. Kivelson and D. E. Heim, *Phys. Rev. B* **26**, 4278 (1982).
- ¹⁹The critical z can be independently estimated by averaging three different extrapolations: for even rings, one extrapolates the crossing point $z^0(\mathcal{N})$; for odd rings and open chains one extrapolates to $\mathcal{N} \rightarrow \infty$ the full \mathcal{E}_G -vs- z curve, then calculates the minimum of the second derivative, $\partial^2 \mathcal{E}_G(\infty)/\partial z^2$. The average of the three results is $z_c = 0.42 \pm 0.04$.
- ²⁰A. Girlando, A. Painelli, and C. Pecile, *Mol. Cryst. Liq. Cryst.* **112**, 325 (1984).
- ²¹In this table the significant digits are those common to the ρ values obtained by extrapolating $\rho(\mathcal{N}, z)$ separately for rings and open chains. These values coincide, within the accuracy of the calculations, with those obtained by applying Eq. (6) directly to the extrapolated $\mathcal{E}_G(\infty, z)$.
- ²²R. E. Peierls, *Quantum Theory of Solids* (Clarendon, Oxford, 1955), Chap. 5.
- ²³P. M. Chaikin, *Ann. N.Y. Acad. Sci.* **313**, 128 (1978); T. D. Schultz, in *The Physics and Chemistry of Low Dimensional Solids*, edited by L. Alcacer (Reidel, Dordrecht, 1980), p. 1.
- ²⁴J. W. Bray, L. V. Interrante, I. S. Jacobs, and J. C. Bonner, in *Extended Linear Chain Compounds*, edited by J. S. Miller (Plenum, New York, 1983), Vol. 3, Chap. 7.
- ²⁵A. Painelli and A. Girlando, *J. Chem. Phys.* **84**, 5665 (1986).
- ²⁶See, for instance, E. H. Lloyd and W. G. Penney, *Trans. Faraday Soc.* **35**, 835 (1939).
- ²⁷E. I. Rashba, in *Excitons*, edited by E. I. Rashba and M. D. Sturge (North-Holland, Amsterdam, 1982), p. 556.
- ²⁸N. O. Lipari, C. B. Duke, and L. Pietronero, *J. Chem. Phys.* **65**, 1165 (1976), and references therein.
- ²⁹M. J. Rice, L. Pietronero, and P. Brüesch, *Solid State Commun.* **21**, 757 (1977); K. Yakushi and H. Kuroda, *Chem. Phys. Lett.* **111**, 165 (1984).
- ³⁰M. Meneghetti, A. Girlando, and C. Pecile, *J. Chem. Phys.* **83**, 3134 (1985).
- ³¹S. N. Dixit and S. Mazumdar, *Phys. Rev. B* **29**, 1824 (1984).
- ³²D. J. Klein and M. A. Garcia-Bach, *Phys. Rev. B* **19**, 877 (1979).
- ³³See, for instance, D. L. Landau and E. M. Lifshitz, *Statistical Physics* (Addison-Wesley, Reading, MA, 1969), paragraphs 83 and 144.
- ³⁴Y. Kamai, M. Tani, S. Kagoshima, Y. Tokura, and T. Toda, *Synth. Metals* **10**, 157 (1984), and references therein.
- ³⁵R. M. Metzger and J. B. Torrance, *J. Am. Chem. Soc.* **107**, 117 (1985).
- ³⁶C. S. Jacobsen and J. B. Torrance, *J. Chem. Phys.* **78**, 112 (1983).